Author(s): Räsänen, E. & Saarikoski, H. & Puska, M. J. & Nieminen, Risto M.

Title: Wigner molecules in polygonal quantum dots: A density-functional study

Year: 2003

Version: Final published version

Please cite the original version:

Räsänen, E. & Saarikoski, H. & Puska, M. J. & Nieminen, Risto M. 2003. Wigner molecules in polygonal quantum dots: A density-functional study. Physical Review B. Volume 67, Issue 3. 035326-1-7. ISSN 1550-235X (electronic). DOI: 10.1103/physrevb.67.035326.

Wigner molecules in polygonal quantum dots: A density-functional study

E. Räsänen, H. Saarikoski, M. J. Puska, and R. M. Nieminen
Laboratory of Physics, Helsinki University of Technology, P.O. Box 1100, FIN-02015 HUT, Finland
(Received 9 August 2002; published 31 January 2003)

We investigate the properties of many-electron systems in two-dimensional polygonal (triangle, square, pentagon, hexagon) potential wells by using the density-functional theory. The development of the ground-state electronic structure as a function of the dot size is of particular interest. First, we show that in the case of two electrons, the Wigner molecule formation agrees with previous exact diagonalization studies. Then we present in detail how the spin symmetry breaks in polygonal geometries as the spin density-functional theory is applied. In several cases with more than two electrons, we find a transition to the crystallized state, yielding coincidence with the number of density maxima and the electron number. We show that this transition density, which agrees reasonably well with previous estimations, is rather insensitive to both the shape of the dot and the electron number.

DOI: 10.1103/PhysRevB.67.035326 PACS number(s): 73.21.La, 71.10.−w

I. INTRODUCTION

Research into nanoscale electronic structures has been expanding continuously. Quantum dots[1] represent basic electron systems that have been fabricated using semiconductor materials for almost 15 years. Because the confinement of electrons in quantum dots or ''artificial atoms'' can be varied at will, they have become a playground in which the basic physics of interacting electrons can be surveyed and theoretical models can be tested.

In quantum dots the correlation effects between electrons have to be considered carefully because the external confinement is remarkably weaker than in real atoms, where the independent electron model with mean-field theories usually gives good results. As the confinement strength is lowered, the mutual Coulomb interaction becomes gradually dominant, and at a certain point, the electron density begins to exhibit localization to classical positions in order to minimize the interaction. This phenomenon corresponds to the Wigner crystallization (WC) in a two-dimensional electron gas (2DEG) (Ref. 2). According to quantum Monte Carlo simulations, the crystallization occurs when the 2D electron density n has decreased such that the density parameter $r_s > 37$. Here $n = 1/(\pi r_s^2)$ and r_s is given in units of the effective Bohr radius $a_B^* = \hbar^2 \epsilon / m^* e^2$, where ϵ is the dielectric constant and m^* is the effective electron mass, specific to the semiconductor material in question. In 2DEG with impurities the broken translational invariance has been shown to result in the WC at a much larger electron density with $r_s \simeq 7.5$ (Ref. 3). In quantum dots the transition to the WC has been predicted to occur at even higher electron densities.[4–8] One of the questions in this context is how the shape and electron number of a two-dimensional quantum dot affect the crystallization.

The weak-confinement limit in quantum dots has been studied with various theoretical methods, including exact diagonalization,[4,9] quantum Monte Carlo[5,10] (QMC), and unrestricted Hartree-Fock[6,8] (UHF) techniques, as well as the spin density-functional theory[7,11–13] (SDFT). In this regime the SDFT allows the formation of spin density waves (SDW's), i.e., the breaking of the spin symmetry,[12] leading to a lower total energy in the system. In our earlier work for a parabolic six-electron quantum dot, we examined the energy difference between the polarized and paramagnetic spin states, and showed that the SDW solution agrees well with the QMC results, in contrast to the symmetry-preserved DFT solution.[11] However, the problem in the SDFT calculations is the fact that only the z component of the total spin can be specified. Therefore, one may ask if a mixed state of several eigenstates, corresponding to different S with a fixed S_z, is physically meaningful, an argument presented by Hirose and Wingreen.[14] In fact, a mixed-symmetry state is not an eigenstate of the Hamiltonian, but the lowest state of a well-defined mixture of symmetries is a functional of the density *at the time of preparation of the state*.[15] The symmetry-broken electron structure thus gives more accurate approximations for the energy and describes the internal nature of the many-body wave function better than the symmetry-preserved solution.[16]

The criterion for the WC in quantum dots may be determined with several attributes. Egger *et al.*[5] considered three criteria yielding similar results in their QMC analysis for parabolic quantum dots. They observed the electron density in real space and searched for the confinement at which the shell structure began to form. In addition, they monitored a quantity depending on the pair-correlation function and changes in the energy spectra. Localization may also be observed directly by examining the probability densities of single electrons.[10] Creffield *et al.*[4] have studied the systems of two electrons confined by polygonal 2D infinite-barrier wells, and their criterion for the onset of the WC is the appearance of a local density minimum at the center of the dot. In the (S)DFT calculations the criterion should be based on the density (spin densities). However, it became evident in our study that the criterion by Creffield *et al.* cannot be applied for polygonal dots containing more than two electrons, because the electron density has maxima at the corners of the dot also at very high electron densities.

Quantum dots are usually modeled by restricting a certain number of electrons to a 2D plane and assuming the confining potential to have a parabolic shape. An example of more general modeling is the above-mentioned exact diagonaliza-

tion study by Creffield *et al.*[4] Moreover, Akbar and Lee[13] used the SDFT to study square quantum dots which have a small finite extent in the third dimension perpendicular to the square. In the case of two electrons, they found good agreement with the results of Creffield *et al.* For two- and four-electron dots, Akbar and Lee estimated the onset of the WC to occur at $r_s \sim 6$.

In the present work we employ the SDFT to investigate the properties of two-dimensional quantum dots with a general polygonal confinement. We concentrate on the WC in the weak-confinement limit, which is obtained simply by increasing the side length of the dot. In the numerical calculations we apply a recently developed real-space approach.[17] As a symmetry-unrestricted method it is flexible regarding the applied geometry and allows also SDW solutions. In the regime of the spin-symmetry-broken solutions, we find that further weakening of the confinement leads to electron densities with as many maxima as there are electrons in the system. We show that the appearance of this behavior can be used, at least in several cases, consistently as a criterion for the onset of the WC for quantum dots of various shapes and different electron numbers.

The outline of the paper is as follows. In Sec. II we present the theoretical model and the computational method of our calculations. From the results we first compare the DFT, i.e., spin-compensated calculations for a two-electron dot to the exact diagonalization results. Then we employ the SDFT and present the symmetry-broken solutions first for a two-electron dot and thereafter for larger systems. A summary and discussion are given in Sec. V.

II. METHODS

The quantum dot material is chosen to be GaAs with the effective electron mass $m^* = 0.067 m_e$ and the dielectric constant $\epsilon = 12.4$. The effective Bohr radius a_B^* is thus 9.79 nm. The Hamiltonian of a many-electron system in a polygonal potential well is written as

$$H = \sum_{i=1}^{N} \left[-\frac{\hbar^2}{2m^*} \nabla_i^2 + V_{\text{ext}}(\mathbf{r}_i) \right] + \sum_{i<j}^{N} \frac{e^2}{\epsilon |\mathbf{r}_i - \mathbf{r}_j|}, \qquad (1)$$

where the external potential has a simple form

$$V_{\text{ext}}(x,y) = \begin{cases} 0, & \text{in the dot,} \\ \infty, & \text{elsewhere.} \end{cases} \qquad (2)$$

The effective mass approximation (EMA) used with the Hamiltonian (1) represents an alternative to the constant-interaction model,[18] in which the Coulomb interaction between the electrons is assumed to be independent of the electron number N. The EMA has been shown to be a reliable approximation if the confinement is not particularly strong.[19]

In the SDFT formalism, the electron density is solved self-consistently with the Kohn-Sham equations.[20,21] To approximate the exchange-correlation energy functional, we use the local spin density approximation (LSDA) with the interpolation form by Tanatar and Ceperley[22] for the 2DEG. Within the EMA, the single-particle Schrödinger equation of the Kohn-Sham scheme reads as

$$\left[-\frac{\hbar^2}{2m^*} \nabla^2 + V_{\text{eff}}^{\sigma}(\mathbf{r}) \right] \psi_{i,\sigma}(\mathbf{r}) = \epsilon_i \psi_{i,\sigma}(\mathbf{r}), \qquad (3)$$

where V_{eff}^{σ} is the effective potential for spin σ containing the external potential and the Hartree and exchange-correlation potentials of the electron-electron interactions. In the spin-compensated calculations (equal spin densities), the scheme reduces to the standard density functional theory within the local density approximation (LDA).

In the self-consistent Kohn-Sham scheme, we perform calculations in real space by using two-dimensional point grids. The number of grid points in the computing region is 80×80. This allows the use of four grids in the employed multigrid scheme (see below) and gives an accuracy better than $\sim 3\%$ in the total energy, checked with Richardson extrapolation.[23] The differential equations are discretized with finite differences,[24] and the procedure is efficiently accelerated with multigrid techniques[25] to solve the Poisson and single-particle Schrödinger equations. Applying the multigrid scheme in the latter case is a fairly complicated task because both the eigenfunctions and eigenvalues have to be solved simultaneously. In order to avoid nonlinearity problems, the Rayleigh quotient multigrid (RQMG) method[26] is used for the solution of the eigenpair corresponding to the lowest eigenvalue. We employ this method with a recent generalization to an arbitrary number of lowest eigenenergy states.[17] The discretized eigenvalue equation is solved by minimizing the Rayleigh quotient $\langle \psi | H | \psi \rangle / \langle \psi | \psi \rangle$ on the *finest* grid, using the coarser grids to remove the lower-frequency components of the error. The technique reduces remarkably the number of relaxation sweeps needed for solving the Schrödinger equation. Other advantages of the real-space solver are its flexibility with the boundary conditions and good suitability for parallel computing.

III. WIGNER CRYSTALLIZATION OF TWO ELECTRONS

First we perform DFT calculations on two-electron polygonal quantum dots by setting the spin densities equal ($n_\uparrow = n_\downarrow$) to prevent the breaking of the spin symmetry. The ensuing total energy with its decomposition to Coulomb, kinetic, and exchange-correlation energies is given in Fig. 1 for a square dot. As predicted, the Coulomb energy becomes increasingly more dominant over the kinetic energy as the side length L of the dot is enlarged and the WC is expected to occur.

The ground-state electron density distributions for the triangular, square, pentagonal, and hexagonal dots at three side lengths $L = 50$, 100, and 400 nm are presented in Fig. 2. In the small dots the electron density is lumped at the center, whereas the large dots represent Wigner-molecule-like behavior, the density being localized near the corners in order to minimize the dominating Coulomb interaction. The localization is seen to depend strongly on the area of the dot. Creffield *et al.*[4] defined the system to be a Wigner molecule, when a local minimum first appears at the center. According

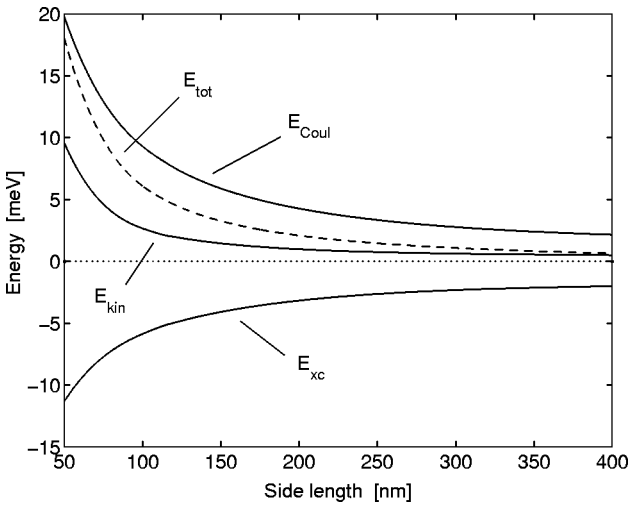

FIG. 1. Energy composition in a square two-electron quantum dot as a function of the dot size.

to our calculations, this occurs in preceding geometries at $L=120$, 80, 60, and 50 nm, respectively, which agree with the exact diagonalization results. This qualitative consistency establishes the applicability of the density-functional approach to small systems considered in this study.

We define the density parameter as $r_s=\sqrt{A/(N\pi)}$, where A is the area of the polygon. In the case of n corners and a side length L we thus get

$$r_s=\frac{L}{2}\sqrt{\frac{n}{N\pi}\cot\frac{\pi}{n}}.$$

By using this definition and applying the criterion presented by Creffield *et al.*[4] for the WC transition point, we find $r_s \sim 3$ for the critical density in all four geometries. Akbar and Lee[13] employed the SDFT for square 2D quantum dots with an additional harmonic confinement along the z axis. They used a more rigorous criterion for the WC, i.e., the breaking of connections between the density maxima, and estimated a critical value of $r_s \sim 6$ for the transition point. Considering their different definitions for the WC, this result is in a qualitative agreement with our $r_s \sim 3$.

Intuitively, the localization of two electrons into all the corners of a polygonal potential well might first appear as a slightly odd result. Jefferson and Häusler[27] have explained the phenomenon with effective charge-spin models. They suggested that the low-energy manifold of a system of strongly correlated electrons can be described properly with an extended single-band Hubbard model. For example, in a square two-electron dot the *tV* Hamiltonian transforms into the following effective Hamiltonian:

$$H_{\text{eff}}=\tilde{E}_0+(\Delta e^{i2\Phi}R_{\pi/2}+\text{H.c.}), \tag{4}$$

where $R_{\pi/2}$ rotates the electrons at opposite corners on a diagonal by $\pi/2$. The electron pair may thus tunnel between the ground-state configurations with an amplitude modulated by a factor $e^{i2\Phi}$. This explains the four-peak structure of the electron density in the Wigner limit, predicted already by Bryant.[28] Diagonalization of H_{eff} gives a good approximation for the ground-state energies obtained from the *tV* Hamiltonian.[29]

IV. SYMMETRY-BROKEN SOLUTIONS

A. Two-electron dot

Next we perform the same calculations as above, but without the restriction $n_\uparrow=n_\downarrow$, and consider still the ground-state solution, for which $S_z=0$. Comparison of the new total energies with the spin-compensated results as a function of the dot size reveals an interesting transition to a lower-energy state. At this point, representing already a Wigner-crystallized distribution, the spin symmetry breaks and the result is a SDW-like ground state.

The relative energy differences between the spin-symmetric and SDW-like solutions, corresponding to our

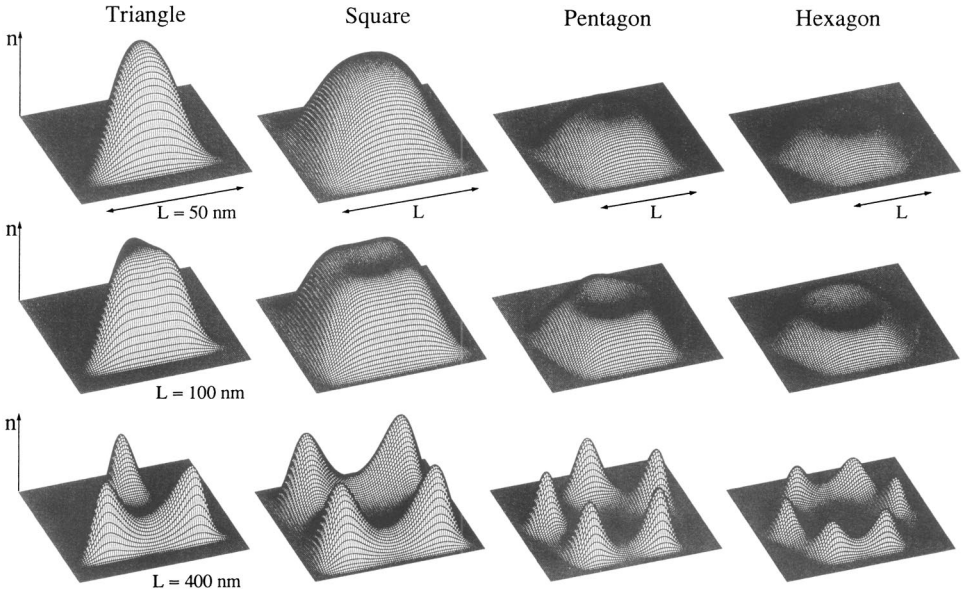

FIG. 2. Electron densities in polygonal two-electron quantum dots with different sizes. In the square, pentagon, and hexagon the amplitudes have been multiplied by a factor of 2.

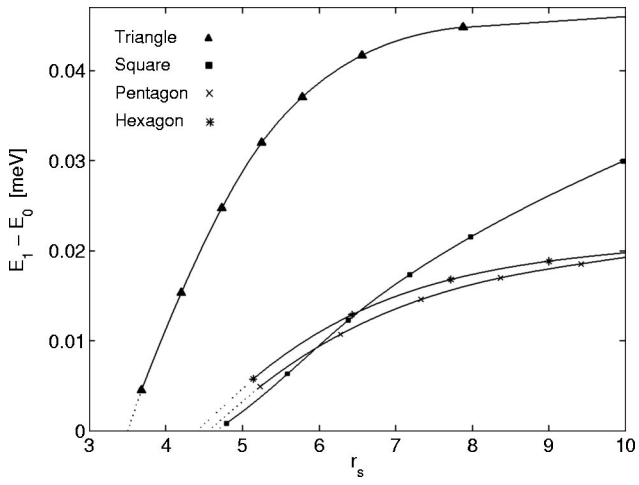

FIG. 3. Total energy differences between the DFT (E_1) and SDFT (E_0) solutions in polygonal two-electron quantum dots of four geometries.

DFT and SDFT calculations, respectively, are shown in Fig. 3 for all the considered geometries. In the triangular well the transition to the symmetry-broken ground state occurs at a remarkably smaller size than in the other three geometries. More precisely, for the triangle we get the transition at $r_s \simeq 3.5$ and for the square, pentagon, and hexagon at $r_s \sim 4.5$.

In order to explain this behavior, one may first examine the lowest Kohn-Sham energy states, shown in Fig. 4 for the triangular and square quantum dots in the symmetry-broken SDFT ground state, as well as in the symmetry-preserved DFT solution. In the latter state, the threefold geometry produces more low-lying degenerate levels in the triangle than the fourfold geometry in the square. In the SDFT calculations these degeneracies are split such that the energy levels become pronouncedly spread in the triangular geometry, whereby the lowest levels are pushed more efficiently downwards in the triangle than in the square, pentagon, and hexagon. There is also a qualitative difference between the symmetry-broken electron densities in these geometries. As

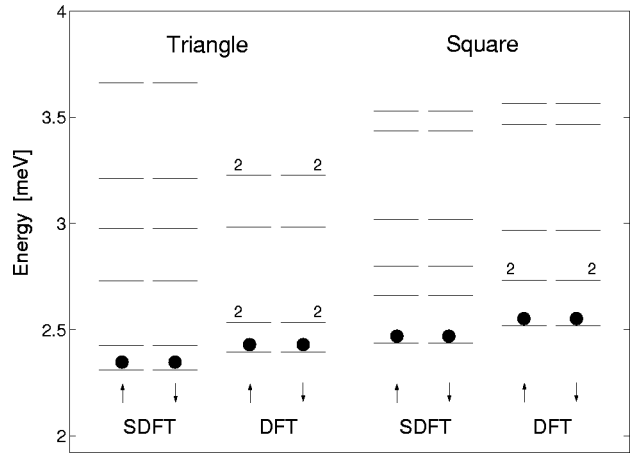

FIG. 4. Lowest Kohn-Sham energy levels of triangular and square two-electron quantum dots at $r_s \sim 8$.

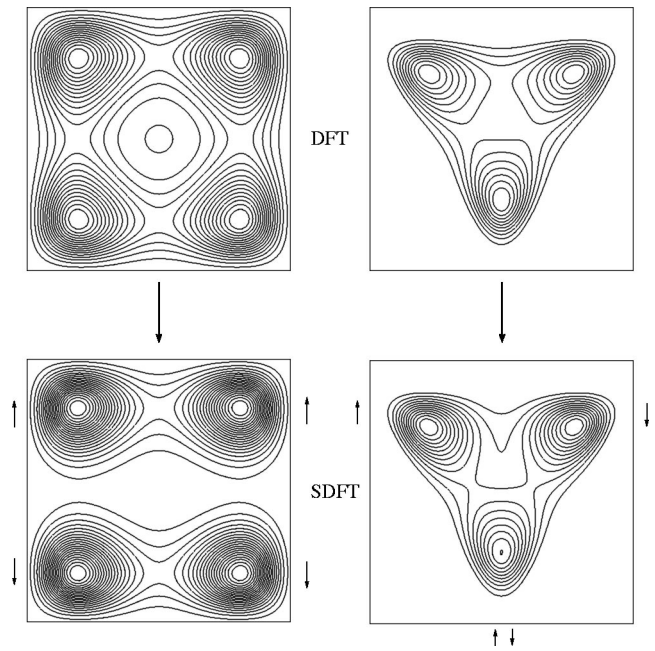

FIG. 5. Difference in the electron densities between the DFT (up) and SDFT (down) solutions in a square and triangular two-electron quantum dot at $L = 400$ nm. The spin alignments are shown in the SDFT case.

shown in Fig. 5, the spin-up and spin-down densities are totally separated in the square, whereas in the triangle they share a corner. In the triangular geometry, the breaking of the spin symmetry can thus lower the energy via the exchange-correlation and Coulomb contributions relatively more and with a relatively smaller cost in kinetic energy than in the square. Nevertheless, in none of these geometries does the breaking of the spin symmetry enlarge the Fermi gap, contrary to SDW formation in large, parabolic quantum dots.[12]

The composition of the energy difference between the symmetry-preserved and the symmetry-broken states is presented in Fig. 6 for a square dot. Naturally, the change in the

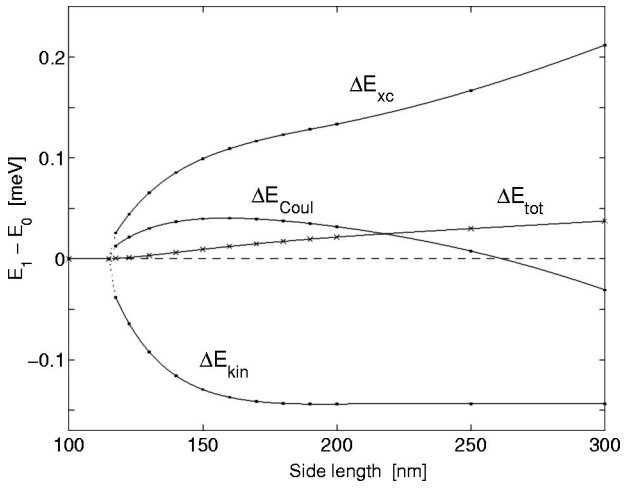

FIG. 6. Composition of the energy difference between the DFT (E_1) and SDFT (E_0) solutions of a square two-electron quantum dot as a function of the dot size.

exchange-correlation energy favors and the change in the kinetic energy opposes the transition. The behavior of the Coulomb energy is interesting: its strong decrease actually initiates the breaking of the spin symmetry. However, as the dot is made larger than $L \sim 250$ nm, the Coulomb energy is higher in the SDW-like than in the symmetry-preserved state. The phenomenon can be understood by having a further look at the electron density distributions in the square as shown in Fig. 5. In the SDFT solution, the electron density is shifted from the region between the opposite spin directions towards the corners. At small dot sizes this decreases the Coulomb repulsion between the charge peaks in the adjacent corners more than the repulsion increases inside the peaks. At large distances the opposite is true.

B. $N>2$

Then we consider some special cases with more than two electrons. The next geometry-independent magic configuration after $N=2$ is a six-electron dot. It represents an interesting point of comparison with the results obtained for a parabolic quantum dot in the weak-confinement limit. We find that the spin symmetry is broken at $r_s \simeq 3.8$, 3.1, 4.6, and 4.9 in triangular, square, pentagonal, and hexagonal quantum dots, respectively.

In the parabolic dot with $V_{\text{ext}}(r) = \frac{1}{2}\omega_0^2 r^2$, the r_s parameter can be estimated from $\omega_0^2 = e^2/(e\pi\epsilon_0\epsilon m^* r_s^3\sqrt{N})$ (Ref. 12). In pursuance of our earlier work for this quantum dot,[11] the SDW formation was not found until $r_s \simeq 6.6$. The sharp corners in the confinement seem thereby favor the transition to the symmetry-broken state. In the six-electron case, however, the triangular geometry is more stable against the transition than the square one. A square with $N=6$ represents an inconvenient combination, similar to the triangle with $N=2$, in which the electrons cannot be evenly divided to the corners of the polygon. As the number of the corners increases further, the transition shifts to higher r_s values, approaching the point of the SDW formation in the parabolic quantum dot with a circular symmetry.

For $N=6$, we consider also the possibility of spin polarization, i.e., the $S_z=3$ state becoming the ground state in the low-density limit. The energy differences between the polarized ($S_z=3$) and paramagnetic ($S_z=0$) states for triangular and square geometries as a function of r_s are shown in Fig. 7. For comparison, the SDFT results for the parabolic quantum dot[11] are also presented, the latter showing spin polarization at $r_s > 12$. We were not able to obtain well-converged results for the triangle and square quantum dots at large r_s values. Therefore we can only speculate by extrapolation that polarization could occur in the triangle and square slightly earlier than in the parabolic quantum dot.

Besides the geometry, we can study how the number of electrons affects the breaking of spin symmetry. First we consider a square dot with $N=6$, 8, and 12, which all correspond to completely filled shells. Figure 8 shows the energy difference between the spin symmetry-preserved and -broken solutions as a function of the r_s. For $N=6$ and $N=12$, the spin symmetry breaks at $r_s \simeq 1.7$ and $r_s \simeq 1.1$, respectively, whereas the ground state of the $N=8$ dot remains

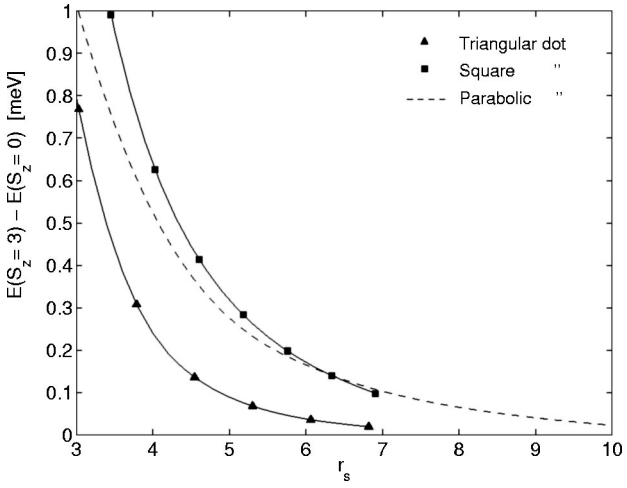

FIG. 7. Total energy differences between the $S_z=3$ and $S_z=0$ states in the triangular (triangle markers), square (square markers), and parabolic (dashed line) six-electron quantum dots.

spin symmetric until $r_s \simeq 2.8$. However, the energy difference grows rapidly in this dot, being considerably larger than in the $N=6$ dot at $r_s \simeq 10$. In the large dots the SDFT solutions show pronounced localization of the spin densities as can be seen in Fig. 9. For $N=6$ and 8, the number of maxima in the total electron densities equals number of electrons, leading to π and $\pi/2$ rotational symmetries in these systems, respectively. The spin symmetry can be considered to be broken more completely in the $N=8$ dot, where the density peaks with the same spin are located on diagonally opposite vertices, in contrast to the $N=6$ dot where they lie on adjacent corners. The interaction is thus minimized more efficiently in the $N=8$ dot, corresponding to a relatively rapid decrease of the total energy shown in Fig. 8. For comparison, the results for a triangular quantum dot with $N=6$ are also presented. In that system, the increase in the energy difference resembles

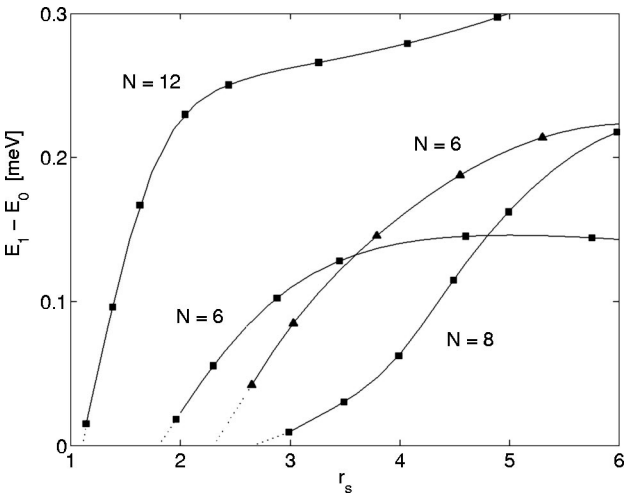

FIG. 8. Total energy differences between the DFT (E_1) and SDFT (E_0) solutions in square quantum dots with $N=6$, 8, and 12 (square markers). Results for the $N=6$ triangle quantum dot are also given (triangle markers).

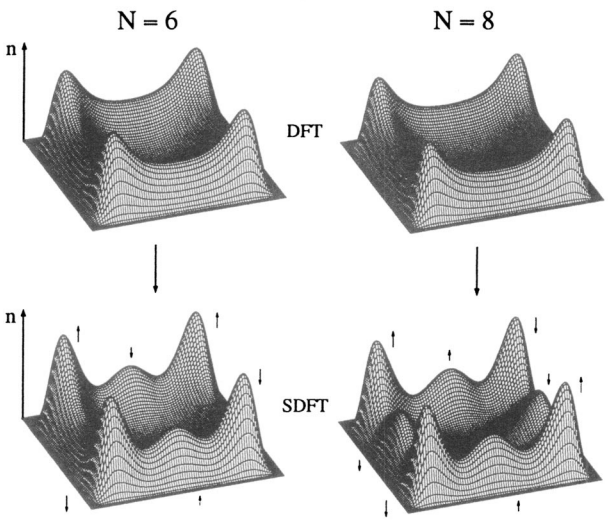

FIG. 9. Electron densities of the DFT (up) and SDFT (down) solutions in $N=6$ and $N=8$ square quantum dots with side lengths $L=300$ nm. The spin alignments are shown in the SDFT case.

the behavior of the $N=8$ square dot, reflecting a similar symmetry-broken geometry (see Fig. 10, below).

After the breaking of the spin symmetry, there can be seen only four density maxima in the corners of the $N=6$ and $N=8$ square quantum dots, resembling the DFT solution (the upper row of Fig. 9). The dot size has to be increased substantially before the maxima in the middle of the edges appear (the lower row). We can observe the same behavior in the $N=6$ triangle and $N=10$ pentagon, in both where the spin symmetry breaks at $r_s \simeq 2.3$. Their density distributions at large r_s values are given in Fig. 10. In all these four cases, the number of density maxima equals the number of electrons in the system. Therefore the appearance of the last density peaks can be considered as the final stage in the onset of the WC in the SDFT formalism.

In order to analyze the appearance of the last density peaks, we show in Fig. 11 the lowest Kohn-Sham energy levels for the $N=6$ square quantum dot with side lengths $L=100$ and 400 nm, corresponding to $r_s \sim 2$ and 9, respectively. At the smaller size, the spin symmetry has already broken and split the DFT degeneracies. As the dot is made larger, the two lowest states become closer to each other and are remarkably lowered in comparison with the symmetry-preserved DFT solution. This condensation occurs similarly

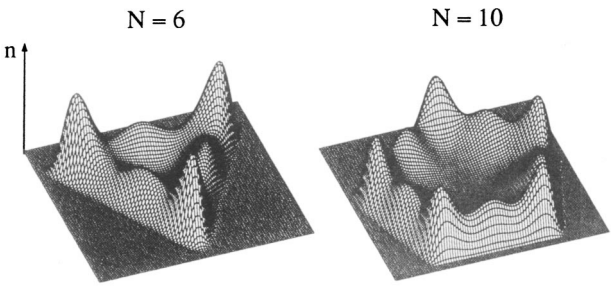

FIG. 10. Electron densities at $r_s \sim 8$ in triangular and pentagonal quantum dots with $N=6$ and $N=10$, respectively.

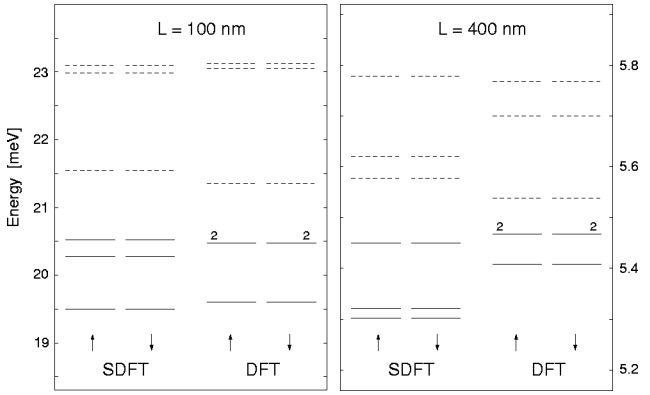

FIG. 11. Lowest Kohn-Sham energy levels in a $N=6$ square quantum dot with side lengths $L=100$ and 400 nm. Solid and dashed lines correspond to the occupied and unoccupied states, respectively. The levels are nondegenerate, except the doubly degenerate levels denoted by the numbers (2).

in all the dots, in which the electron density localizes to a number of maxima coinciding with the number of electrons. The appearance of the last density maxima thus drives the lowest Kohn-Sham energy levels towards degeneracy. The complete degeneracy would be the ultimate state for the Wigner crystal. In Fig. 11 one can also notice that the Fermi gap is considerably larger in the symmetry-broken solution than in the symmetry-preserved case, resembling the situation in large, parabolic quantum dots.[12]

We have carefully determined the r_s values at which the last maxima appear and found astonishingly similar values for the different systems studied, although the breaking of the spin symmetry occurs on a broad r_s scale. The critical values of r_s are $\simeq 3.8$ and 4.0 for $N=6$ and $N=8$ square dots, respectively, and $r_s \simeq 3.9$ for both the $N=6$ triangle and the $N=10$ pentagon. In the case of two-electron dots, the above criterion for the WC cannot be applied, but the onset of the spin-symmetry-broken state gives a reasonable estimate of $r_s \simeq 3.5$ for the triangular $N=2$ dot and $r_s \simeq 4.5$ for the other $N=2$ polygonal quantum dots. Our estimate of $r_s \simeq 4.0$ for the WC transition point is consistent with the results for small, parabolic quantum dots.[5–12] It is also clearly smaller than $r_s \simeq 7.5$ obtained for the fluid-solid transition in 2DEG containing impurities.[3]

V. SUMMARY

We have studied the electronic properties of polygonal two-dimensional quantum dots by employing the spin density-functional theory. The numerical calculations are performed with a symmetry-unrestricted real-space scheme. Especially, we have focused on the behavior of these systems at the weak-confinement limit, where the role of the electron-electron interactions becomes dominating and eventually leads to the formation of the so-called Wigner molecules.

First we have shown that the density-functional theory is capable of reproducing, in agreement with the exact diagonalization studies, the behavior of the electron density in polygonal two-electron quantum dots as the spatial size of the potential well increases.

The spin density-functional theory leads inevitably to the breaking of the spin symmetry. For different geometries and different electron numbers, this occurs in a wide range of average electron densities or r_s parameters. The spin-symmetry-broken density shows for certain geometries and electron numbers a gradual transition, such that the number of density maxima coincides with the number of electrons. We use the appearance of the last density maxima as the criterion for the Wigner crystallization and obtain $r_s \simeq 4.0$ for the critical density. This value does not depend strongly on the geometry nor the electron number of the quantum dot and is in agreement with quantum Monte Carlo results.

ACKNOWLEDGMENT

This research has been supported by the Academy of Finland through its Centers of Excellence program (2000-2005).

[1] R.C. Ashoori, Nature (London) **379**, 413 (1996).
[2] E.P. Wigner, Phys. Rev. **46**, 1002 (1934).
[3] S.T. Chui and B. Tanatar, Phys. Rev. Lett. **74**, 458 (1995).
[4] C.E. Creffield, W. Häusler, J.H. Jefferson, and S. Sarkar, Phys. Rev. B **59**, 10 719 (1999).
[5] R. Egger, W. Häusler, C.H. Mak, and H. Grabert, Phys. Rev. Lett. **82**, 3320 (1999).
[6] C. Yannouleas and U. Landman, Phys. Rev. Lett. **82**, 5325 (1999).
[7] S.M. Reimann, M. Koskinen, and M. Manninen, Phys. Rev. B **62**, 8108 (1999).
[8] B. Reusch, W. Häusler, and H. Grabert, Phys. Rev. B **63**, 113313 (2001).
[9] S.A. Mikhailov, Phys. Rev. B **65**, 115312 (2002).
[10] A. Harju, S. Siljamäki, and R.M. Nieminen, Phys. Rev. B **65**, 075309 (2002).
[11] H. Saarikoski, E. Räsänen, S. Siljamäki, A. Harju, M. Puska, and R.M. Nieminen, Eur. Phys. J. B **26**, 241 (2002).
[12] M. Koskinen, M. Manninen, and S.M. Reimann, Phys. Rev. Lett. **79**, 1389 (1997).
[13] S. Akbar and I.H. Lee, Phys. Rev. B **63**, 165301 (2001).
[14] K. Hirose and N.S. Wingreen, Phys. Rev. B **59**, 4604 (1999).
[15] U. von Barth, Phys. Rev. A **20**, 1693 (1979).
[16] M. Koskinen, M. Manninen, B. Mottelson, and S.M. Reimann, Phys. Rev. B **63**, 205323 (2001).
[17] M. Heiskanen, T. Torsti, M.J. Puska, and R.M. Nieminen, Phys. Rev. B **63**, 245106 (2001).
[18] L.P. Kouwenhoven and C. Marcus, Phys. World **11**, 35 (1998).
[19] A. Franceschetti and A. Zunger, Phys. Rev. B **62**, 2614 (2000).
[20] P. Hohenberg and W. Kohn, Phys. Rev. **136**, B864 (1964).
[21] W. Kohn and L.J. Sham, Phys. Rev. **140**, A1133 (1965).
[22] B. Tanatar and D.M. Ceperley, Phys. Rev. B **39**, 5005 (1989).
[23] W.H. Press, B.P. Flannery, S.A. Teukolsky, and W.T. Vetterling, *Numerical Recipes in FORTRAN* (Cambridge University Press, Cambridge, England, 1992).
[24] T.L. Beck, Rev. Mod. Phys. **72**, 1041 (2000).
[25] A. Brandt, Math. Comput. **31**, 333 (1977).
[26] J. Mandel and S. McCormick, J. Comput. Phys. **80**, 442 (1989).
[27] J.H. Jefferson and W. Häusler, Phys. Rev. B **54**, 4936 (1996).
[28] G.W. Bryant, Phys. Rev. Lett. **59**, 1140 (1987).
[29] C.E. Creffield, J.H. Jefferson, S. Sarkar, and D.L.J. Tipton, Phys. Rev. B **62**, 7249 (2000).